

Time-Reversal Coherent Control in Nanoplasmonics

Xiangting Li^{1,2,*} and Mark I. Stockman^{1,†}

¹*Department of Physics and Astronomy, Georgia State University, Atlanta, GA 30303, USA*

²*Department of Physics, Shanghai Jiaotong University, Shanghai 200240, China*

(Dated: November 5, 2018)

We introduce an approach to determining the required waveforms to coherently control the optical energy localization in plasmonic nanosystems. This approach is based on the impulsive localized excitation of the nanosystem and time reversal of the generated far-zone field at a single point with one polarization. Despite strong interaction and significant dephasing and dissipation in metal plasmonic systems, and incompleteness of this time reversal, the proposed approach proves to be very efficient in controlling the nanoscale optical fields. Possible applications include nanoscale spectroscopy and photomodification, ultradense memory, and information processing on the nanoscale.

PACS numbers: 78.67.-n, 71.45.Gm, 42.65.Re, 73.20.Mf

One of the challenging problems is control of the nanoscale localization of optical excitation energy in nanosystems. The principal physical origin of this problem is that the wavelength of the optical radiation is orders of magnitude larger than the size of a nanoscale system. Therefore the optical radiation cannot be focused into a nanoscale spot, i.e., it does not possess spatial degrees of freedom on the nanoscale. However, it does possess the temporal degrees of freedom, which is the same, in a different language, as the frequency or phase degrees of freedom. The idea to use the phase modulation of the optical radiation to control the nanoscale localization of the optical energy has been proposed¹ and led to a significant subsequent development both theoretical^{2,3,4,5} and experimental^{6,7}. In symmetric systems, polarization of the excitation has been an efficient degree of freedom complementing the phase and amplitude modulation.^{4,5,7} Coherent control of quantum and nanoscopic systems is a powerful tool of defining pathways of optically-excited processes in them.^{8,9,10,11,12,13}

One of the fundamental problems in the coherent control is the solution of its “inverse problem”: finding an optical waveform that sends the controlled system along the required excitation pathway. One approach to this problem is the adaptive optimum control that has proved successful in a wide class of problems.^{5,7,10,11} However, in the adaptive algorithms, it is sometimes difficult to interpret the obtained complicated waveforms. A problem in theoretical investigations is that implementations of the adaptive algorithms are often computationally costly.

In this Letter we propose and theoretically investigate a novel approach to finding an efficient optical pulse controlling a nanosystem. It is based on an idea of time reversal (or, back propagation). We start with an initial state of the plasmonic nanosystem where a localized excitation is prepared at a desired nanosite. Then we solve the direct problem of evolution and propagate the fields to the far zone. At some moment t_r , we time-reverse the far-zone pulse and send it back to the system. If the system were completely time reversible, then its evolution would back-track itself causing the concentration of energy at the desired site in time t_r after the instance of

the time reversal. This idea is significantly based on the previous acoustic and microwave studies.^{14,15,16}

However, there are principal differences of surface plasmon (SP) eigenmodes in metal nanosystems from the reverberating, leaky modes in acoustics and microwaves of Refs. 14,15,16, which make controlling the SPs much more difficult. First, due to the strong interaction of dipolar excitations on the nanoscale, the SPs in nanosystems form chaotic eigenmodes that can be delocalized over the entire nanosystem.^{17,18} This phenomenon manifests itself as correlated “hot spots” of local fields. Obviously, both the delocalization of the SPs and their chaoticity (including high sensitivity to parameters) hamper the ability to control them. Second important difference is that the real metals in the plasmonic spectral region are lossy.¹⁹ Therefore, SPs have finite life times and are not exactly time-reversible. The third problem, which is common to the acoustics, microwaves, and plasmonics, is that the far field does not contain the full information of the internal state of the systems: the evanescent fields are vanishingly small and lost in the far zone. Moreover, the far-zone field is normally measured in a limited number of points with incomplete polarization information (in the extreme case, at one point with a single polarization). Therefore, the full time-reversal of the field is impossible. These serious problems notwithstanding, as we show below in this Letter, the time reversal of the far-zone field even at a single point with a single polarization produces a signal that is capable of providing an excellent control of the optical field nano-localization.

Turning to the theory, we consider a nanostructured system consisting of metal and dielectric with the permittivities ε_m and ε_d , respectively. The entire size of this system is assumed to be much less than the wavelength of the excitation radiation. Therefore we can use the quasistatic spectral theory.^{2,20} We start with an optical dipole $\mathbf{d}(\mathbf{r}_0, t)$ localized at a point \mathbf{r}_0 at the metal surface whose density is $\mathbf{P}(\mathbf{r}) = \delta(\mathbf{r} - \mathbf{r}_0)\mathbf{d}(\mathbf{r}_0, t)$, and the dependence on time t is a short pulse containing frequencies ω centered around the carrier frequency ω_0 .

This initial oscillating dipole causes the appearance of

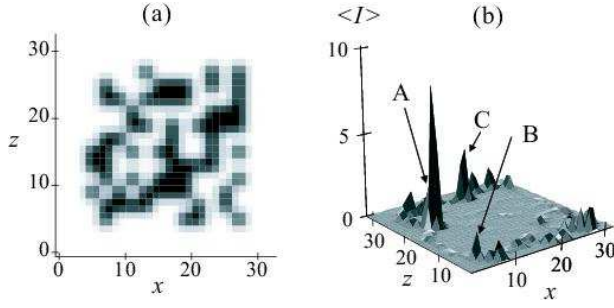


FIG. 1: (a) Geometry of the random planar composite used in the computations, shown in the xz projection. The unit length for the axes is 1 nm, but can be scaled. The system is scalable in the limits allowed by the quasistatic approximation. (b) Average (over pulse time) intensity of local fields is displayed distributed over the surface of the nanosystem. The fields magnitude is shown in the units of the excitation pulse amplitude, which is set as 1, and whose length is 5 fs with mean frequency $\omega_0 = 1.2$ eV.

local fields $\mathbf{E}^L(\mathbf{r}, t)$ in the system that are given by²¹

$$E_{\alpha}^L(\mathbf{r}, \omega) = \frac{4\pi}{\varepsilon_d} G_{\alpha\beta}^r(\mathbf{r}, \mathbf{r}_0; \omega) d_{\beta}(\mathbf{r}_0, \omega), \quad (1)$$

where the Greek subscripts denote vector indices with summation over repeated indices implied. Here and below, by indicating a frequency variable ω we imply the Fourier transform of the corresponding temporal function; e.g., $\mathbf{E}(\mathbf{r}, \omega) = \int_{-\infty}^{\infty} \mathbf{E}(\mathbf{r}, t) \exp(i\omega t) dt$. Retarded dyadic Green's function $G_{\alpha\beta}^r$ is expressed in terms of the corresponding scalar Green's function \bar{G}^r :

$$G_{\alpha\beta}^r(\mathbf{r}, \mathbf{r}'; \omega) = \frac{\partial^2}{\partial r_{\alpha} \partial r'_{\beta}} \bar{G}^r(\mathbf{r}, \mathbf{r}'; \omega). \quad (2)$$

This is given as an expansion over the eigenfunctions φ_n and eigenvalues s_n of the SP eigenproblem^{2,20,21}

$$\bar{G}^r(\mathbf{r}, \mathbf{r}'; \omega) = \sum_n \frac{\varphi_n(\mathbf{r}) \varphi_n(\mathbf{r}')^*}{s(\omega) - s_n}, \quad s(\omega) = \frac{\varepsilon_d}{\varepsilon_d - \varepsilon_m}. \quad (3)$$

The total radiating dipole moment of the nanosystem \mathbf{D} , which defines the field in the far zone, is the seed dipole \mathbf{d} plus the dipole of the entire system induced by field \mathbf{E}^L (1) that renormalizes and enhances it (the antenna effect). It is given in the frequency domain as²¹

$$D_{\alpha}(\omega) = \left[\delta_{\alpha\beta} - \frac{1}{s(\omega)} g_{\beta\alpha}(\mathbf{r}_0; \omega) \right] d_{\beta}(\mathbf{r}_0, \omega), \quad (4)$$

$$g_{\alpha\beta}(\mathbf{r}, \omega) = \int_V G_{\alpha\beta}^r(\mathbf{r}, \mathbf{r}'; \omega) \Theta(\mathbf{r}') d^3 r', \quad (5)$$

where $\Theta(\mathbf{r}')$ is the characteristic function equal to 1 when \mathbf{r}' belongs to the metal and to 0 otherwise. To complete

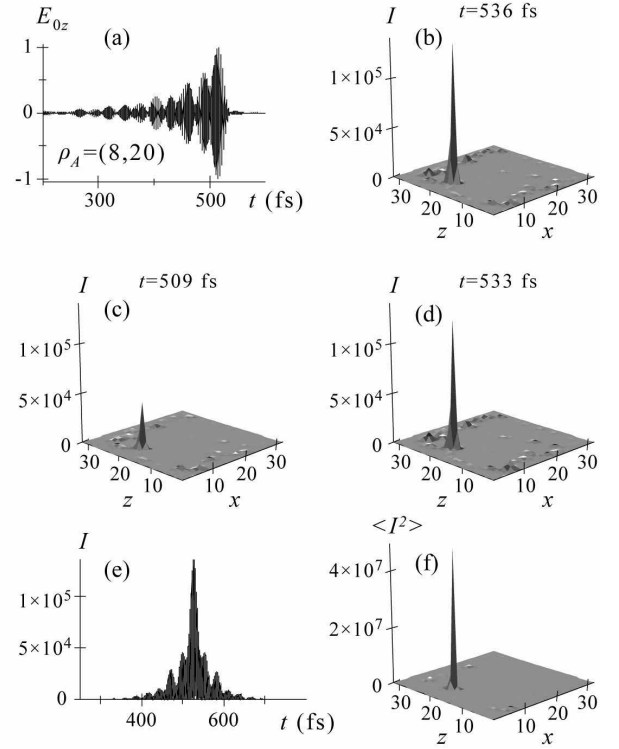


FIG. 2: (a) Excitation field at the system as computed by time-reversal for the initial dipole at the A point (normalized to 1 at the maximum). (b)-(d) Distributions of the local field intensity at the points A, B, and C, correspondingly, calculated for the instances of their respective maxima. (e) Time evolution of the local intensity at the targeted point A. (f) Distribution of the time-averaged squared intensity over the surface of the nanosystem. Units of field and intensity are arbitrary but consistent for all the panels.

the solution of the inverse problem of the coherent control, we find the time-reversed radiating dipole moment

$$\mathbf{D}^T(t) = \int_{-\infty}^{\infty} D^*(\omega) \exp(-i\omega t) d\omega / (2\pi). \quad (6)$$

The field generated by this oscillating dipole in the far zone is then used to excite the nanosystem.

The final step is the solution of the direct problem, i.e. finding the local field $\mathbf{E}(\mathbf{r}, t)$ in the system that is excited by the time-reversed *uniform* field $\mathbf{E}^T(t)$. This can be expressed in the Fourier domain as

$$E_{\alpha}(\mathbf{r}, \omega) = [\delta_{\alpha\beta} + g_{\alpha\beta}(\mathbf{r}, \omega)] E_{\beta}^T(\omega). \quad (7)$$

If the time-reversal is efficient in solving the inverse problem, then the local field, Fourier-transformed to the time domain, should demonstrate the concentration at the initial site \mathbf{r}_0 in time t_r after the reversal.

As a numerical illustration, we consider a random planar composite which is a 4-nm thick layer of silver¹⁹ in vacuum. This layer is 50 percent randomly filled with $2 \times 2 \times 2$ nm³ unit cells, as shown in Fig. 1 (a). The

total size of this composites is $32 \times 4 \times 32 \text{ nm}^3$. In the quasistatic approximation, the system is scalable, as long as its total size is still much less the light wavelength.

There are *a priori* limitations on the coherent control in the plasmonic nanosystems. In particular, the local field energy can only be localized at the sites where the eigenmodes with frequencies within the bandwidth of the excitation pulse are localized. To get an idea where in the nanosystem such a localization takes place, we apply a very short, 5-fs duration, unmodulated Gaussian excitation pulse whose carrier frequency $\omega_0 = 1.2 \text{ eV}$ is in the window of the least dephasing of the SPs.²² The resulting local field intensity averaged over the pulse time, is shown in Fig. 1 (b). Among the many hot spots of the local fields seen in this panel, we choose three peaks marked as A, B, and C, whose $\rho = (x, z)$ coordinates at the surface are $\rho_A = (8, 20)$, $\rho_B = (5, 5)$, and $\rho_C = (20, 28)$, correspondingly. In all cases the time dependence of the initial dipole $\mathbf{d}(\mathbf{r}_0, t)$ has been set as a pulse with a 20 fs Gaussian envelope and $\omega_0 = 1.2 \text{ eV}$. The initial dipole was polarized in the z -direction. Separate computations for this dipole x -polarized have given very similar results (not shown), which is due to the strong depolarization effect of the present random nanostructure. This property of random, complex nanosystems is in sharp contrast to the polarization-driven control for a symmetric system.⁷ The time-reversed excitation field in the far zone has been calculated from the dipole (6). Its maximum amplitude on the system has been normalized to 1 to make the comparison of the plasmonic enhancements easier.

When the initial dipole is at the point A, the calculated time-reversed electric field incident on the system is shown in Fig. 2 (a) where $t_r = 536 \text{ fs}$. We can see that this field is dramatically different from the seed 20-fs Gaussian-envelope polarization that generated it (after the time reversal). The pulse is relatively long, with bursts of fields and their revivals, accompanied by the general decay due to the dephasing. This pulse looks very similar to the pulses obtained by the time reversal in acoustics and microwaves^{14,15,16} where this behavior is due the reverberations of the propagating waves repeatedly reflected from the boundaries and inhomogeneities of the system; the decay of the signal is due to the leakage of the wave energy from those open systems. However, the similarity stops here, because in our case the observed beatings are due to the interference of the localized, non-propagating (quasistatic) SPs eigenmodes; the decay is due to their dephasing occurring both due to the multitude and randomness of the eigenmode frequencies involved, and also due to the dephasing of the metal electron polarization as described by $\text{Im} \epsilon_m$.

In Figs. 2 (b)-(d) we display the local field intensity $I(\mathbf{r}, t) = |\mathbf{E}(\mathbf{r}, t)|^2$ distributed over the surface of the nanosystem for three moments of time where the intensities at sites A, B, and C are maximum, correspondingly. Note that in all these cases the initial dipole is at the A point. The maximum concentration of energy at the A site is almost perfect [panel (b)]; it is reached at $t = 536$

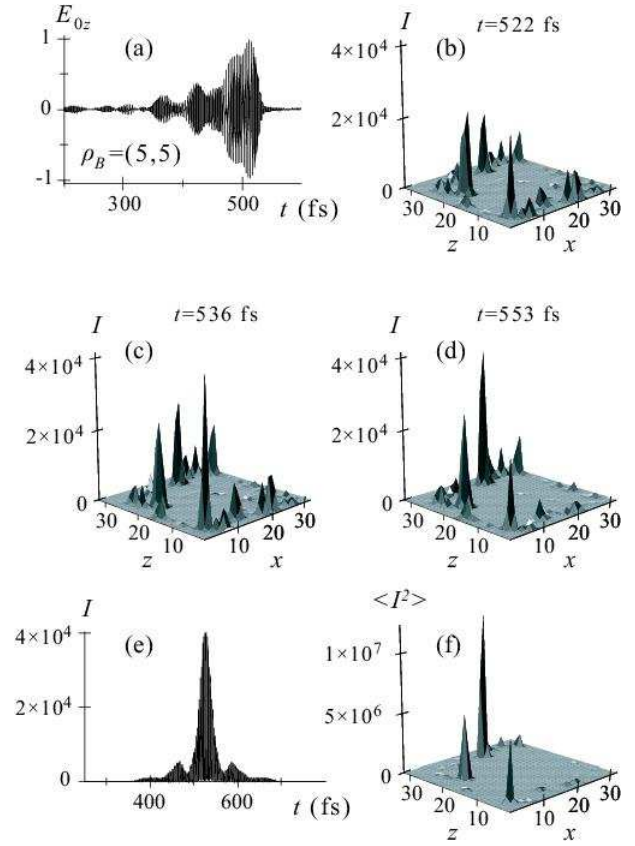


FIG. 3: The same as in Fig. 2 but for the initial dipole at the B point.

fs, which coincides with the expected time t_r (the end of the excitation pulse). Comparing to the case of an unmodulated pulse [Fig. 1 (b)], the excitation of the other peaks is almost completely suppressed. Even when the “undesired” peaks B and C go through their temporal maxima [panels (c) and (d)], the targeted peak A is still dominant. Not only the spatial structure of the local fields is highly concentrated. Also the temporal evolution of the local field intensity at the A point shown in Fig. 2 (e) is restored almost completely to its initial Gaussian envelope (though with some pedestal). Finally, we display in Fig. 2 (f) the time-integrated square of the intensity, which describes the distribution of the two-photon electron-emission current as measured, e. g., by a photoemission electron microscope (PEEM).^{6,7} Such a current is almost ideally concentrated at the targeted point A.

Similar case for the initial dipole at the B point is illustrated in Fig. 3. The excitation, time-reversed pulse [panel (a)] is significantly different from the previous case: the beatings are obviously much less frequent. The spatial distributions of the local field intensity displayed in panels (b)-(d) reveal that the initially weak peak B [cf. Fig. 1 (b)] is relatively very much enhanced. It reaches its maximum [panel (c)] at $t = 536 \text{ fs}$ coinciding with the expected (back-tracking) time t_r , where it is the largest peak]. This is certainly a success of the coherent control.

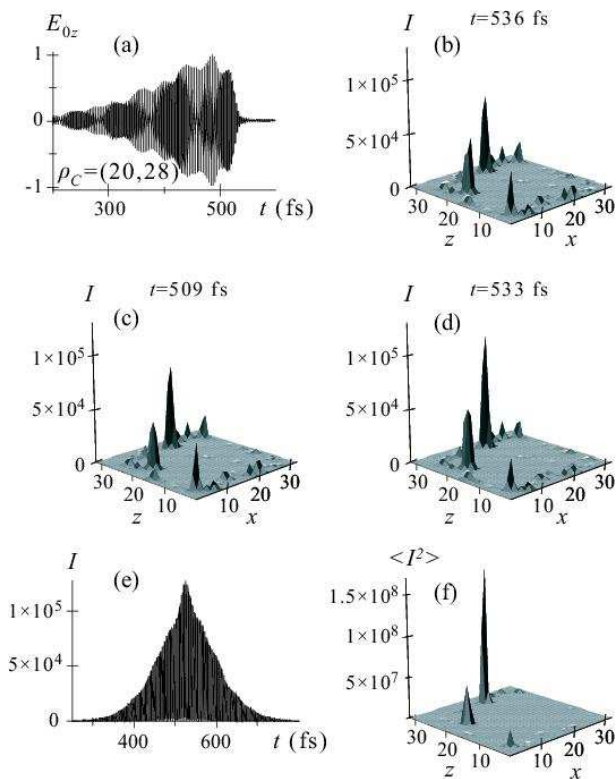


FIG. 4: The same as in Fig. 2 but for the initial dipole at the C point.

Moreover, the time evolution of the local fields at the B site [panel (e)] shows an excellent temporal concentration and reproduction of the seed 20 fs Gaussian pulse. However, as panel (d) shows, the maximum magnitude of the peak at the C site is comparable, though smaller, than that of the maximum B peak. It is also important that the initially strongest peak A [Fig. 1 (b)] is significantly suppressed. The time-averaged nonlinear current [panel (f)] is nevertheless dominated by the C site, which is due to the very long-lived local fields at that site. Thus the temporal concentration at the targeted point B driven by the time-reversed field is sharp and transient in time.

For the C point as targeted, illustrated in Fig. 4, the excitation, time-reversed pulse [panel (a)] is very long, lacking strong beatings, which implies a weak dephasing. The C peak certainly dominates the temporal dynamics reaching its maximum panel (d)] at $t = 533$ fs, which is just one period of oscillations shifted from the back-tracking time $t_r = 556$ fs. The C peak also dominates the nonlinear current [panel (f)]. The temporal dynamics at the targeted C point [panel (e)] shows a rather broadened peak, but its very center exhibits some narrow spike at $t \approx t_r$. Overall, the time-reversal coherent control is very efficient at the selective concentration of the excitation energy at this point.

To briefly conclude, we have introduced an efficient approach to solving an important and formidable problem of the coherent control of the local optical energy distribution in plasmonic nanosystems. We have start with a localized dipole producing a short pulse of optical oscillations at a targeted site of the nanosystem. The field of this dipole with one polarization at a single point in the far zone is time-reversed and used as an excitation pulse. We have shown above that despite the significant problems in time reversing a lossy, strongly interacting plasmonic nanosystems using incomplete information, it is still possible to efficiently concentrate the energy of ultrafast optical fields at the targeted nano-site. Thus, the time reversal provides a powerful method to solve this fundamental problem of the coherent control. This method can be used either as an alternative to or in combination with the adaptive coherent control where it provides the initial pulse. This proposed approach can be used for controlling the ultrafast local optical dynamics in nanosystems for a variety of applications, including superdense and ultrafast optical memory and computing on the nanoscale, ultrafast local spectroscopy and photochemistry on the nanoscale, and others.

This work was supported by grants from the Chemical Sciences, Biosciences and Geosciences Division of the Office of Basic Energy Sciences, Office of Science, U.S. Department of Energy, a grant CHE-0507147 from NSF, and a grant from the US-Israel BSF.

* Electronic address: xiangtingli@yahoo.com

† Electronic address: mstockman@gsu.edu;
URL: <http://www.phy-astr.gsu.edu/stockman>

¹ M. I. Stockman, S. V. Faleev, and D. J. Bergman, Phys. Rev. Lett. **88**, 067402 (2002).

² M. I. Stockman, D. J. Bergman, and T. Kobayashi, Phys. Rev. B **69**, 054202 (2004).

³ M. I. Stockman and P. Hewageegana, Nano Lett. **5**, 2325 (2005).

⁴ T. Brixner, F. J. G. d. Abajo, J. Schneider, and W. Pfeiffer, Phys. Rev. Lett. **95**, 093901 (2005).

⁵ M. Sukharev and T. Seideman, J. Chem. Phys. **124**, 144707 (2006).

⁶ A. Kubo, K. Onda, H. Petek, Z. Sun, Y. S. Jung, and H. K. Kim, Nano Lett. **5**, 1123 (2005).

⁷ M. Aeschlimann, M. Bauer, D. Bayer, T. Brixner, F. J. G. d. Abajo, W. Pfeiffer, M. Rohmer, C. Spindler, and F. Steeb, Nature **446**, 301 (2007).

⁸ G. Kurizki, M. Shapiro, and P. Brumer, Phys. Rev. B **39**, 3435 (1989).

⁹ P. Brumer and M. Shapiro, Annu Rev Phys Chem **43**, 257 (1992).

¹⁰ H. Rabitz, R. de Vivie-Riedle, M. Motzkus, and K. Kompa, Science **288**, 824 (2000).

¹¹ J. M. Geremia and H. Rabitz, Phys. Rev. Lett. **89**, 263902 (2002).

- ¹² N. A. Nguyen, B. K. Dey, M. Shapiro, and P. Brumer, J. Phys. Chem. A **108**, 7878 (2004).
- ¹³ M. Shapiro and P. Brumer, Physics Reports **425**, 195 (2006).
- ¹⁴ A. Derode, A. Tourin, J. de Rosny, M. Tanter, S. Yon, and M. Fink, Phys. Rev. Lett. **90**, (2003).
- ¹⁵ G. Lerosey, J. de Rosny, A. Tourin, A. Derode, G. Montaldo, and M. Fink, Phys. Rev. Lett. **92**, 193904 (2004).
- ¹⁶ G. Lerosey, J. de Rosny, A. Tourin, and M. Fink, Science **315**, 1120 (2007).
- ¹⁷ M. I. Stockman, Phys. Rev. Lett. **79**, 4562 (1997).
- ¹⁸ M. I. Stockman, Phys. Rev. E **56**, 6494 (1997).
- ¹⁹ P. B. Johnson and R. W. Christy, Phys. Rev. B **6**, 4370 (1972).
- ²⁰ M. I. Stockman, S. V. Faleev, and D. J. Bergman, Phys. Rev. Lett. **87**, 167401 (2001).
- ²¹ M. I. Stockman, in *Surface Enhanced Raman Scattering – Physics and Applications*, Springer Series Topics in Applied Physics, edited by M. M. K. Kneipp and H. Kneipp (Springer-Verlag, Heidelberg New York Tokyo, 2006), pp. 47–66.
- ²² D. J. Bergman and M. I. Stockman, Phys. Rev. Lett. **90**, 027402 (2003).
- ²³ H. Rabitz, Science **299**, 525 (2003).